

Performance of 3D differential operators for the detection of anatomical point landmarks in MR and CT images

Thomas Hartkens*, Karl Rohr, H. Siegfried Stiehl

Cognitive Systems Group, Department of Computer Science, University of Hamburg,
Vogt-Kölln-Str. 30, D-22527 Hamburg, Germany

ABSTRACT

Point-based registration of images generally depends on the extraction of suitable landmarks. Recently, different 3D operators have been proposed in the literature to detect anatomical point landmarks in 3D images. While the *localization* performance of 3D operators has already been investigated (e.g., Frantz et al.⁷), studies on the *detection* performance of 3D operators are hardly known. In this paper, we investigate nine 3D differential operators for the detection of 3D point landmarks in MR and CT images. These operators are based on either first, second, or first and second order partial derivatives of an image. In our investigation we use measures, which reflect different aspects of the detection performance of the operators. In the first part of the investigation, we analyze the number of corresponding detections in 3D tomographic images, and in the second part we use statistical measures to determine the detection performance w.r.t. certain landmarks. It turns out that i) operators based on only first order partial derivative of an image yield a larger number of corresponding points than the other operators and that ii) their performance on the basis of the statistical measures is better.

1. INTRODUCTION

The registration of tomographic images is important for diagnosis and surgery planning. One possibility to match two images is to find corresponding points and to use them for calculation of the transformation. As corresponding points we here consider point landmarks in tomographic images, i.e. prominent points, where the surface of anatomical structures is strongly curved, e.g. the tip of the frontal horn of the ventricular system. Usually, such 3D landmarks are manually selected – a task which is tedious, time-consuming, and often lacks accuracy. An alternative is a semi-automatic procedure for landmark selection which has the advantage that the user can interactively control the results. First, an approximate position of a specific landmark is manually determined. Second, to extract potential landmark candidates, a 3D operator is applied within a region-of-interest (ROI) around the approximate position. Third, the user selects the most promising candidate.

In this paper, we investigate nine 3D differential operators for the detection of 3D point landmarks in MR and CT images. These operators are based on either first, second, or first and second order partial derivatives of an image. The main questions of our investigation are: 1. Which operators yield the largest number of corresponding points?, and 2. Which operators detect the landmarks most reliably? To answer these questions, we introduce quantitative measures which represent different aspects of the detection performance. First, we determine the number of corresponding points in images under elastic deformations and noise. Second, we use statistical measures to determine the detection performance for the landmarks within ROIs. We present experimental results for 3D synthetic and 3D tomographic images. Altogether each of the nine operators has been applied to 308 synthetic 3D images (tetrahedra, ellipsoids, and hyperbolic paraboloids with different levels of noise and deformations) and 301 tomographic images (3D subimages of MR- and CT images also with different levels of noise and deformations). Alternative studies on the performance of 3D landmark operators are based on the number of matched points under rigid transformations¹⁴ or determine the rigid or affine registration accuracy.^{14,2} Also, these studies are less comprehensive and only a relatively small number of operators has been considered.

The organization of this paper is as follows: First, we describe the nine investigated differential operators (Sec.2). Then we introduce measures for two aspects of the detection performance (number of corresponding points and statistical measures), which we use to compare the operators (Sec.3). The parameter settings of the investigation and the used image data are described in Sec.4. The experimental results are presented in Sec.5-7, which also include an analysis of the operator values for a 3D synthetic and a 3D tomographic image.

* Email: hartkens@informatik.uni-hamburg.de

Approach "Mean curvature" ^{8,3,5,13,11}		
• $H =$	$\frac{1}{2 \nabla g ^3} [g_x^2(g_{yy} + g_{zz}) + g_y^2(g_{xx} + g_{zz}) + g_z^2(g_{xx} + g_{yy}) - 2(g_x g_y g_{xy} + g_x g_z g_{xz} + g_y g_z g_{yz})]$	
• $Kitchen\&Rosenfeld3D =$	$k_H \cdot 2 \nabla g $	
• $Blom3D =$	$k_H \cdot 2 \nabla g ^3$	with $\nabla g = (g_x, g_y, g_z)^T$
Approach "Gaussian curvature" ^{5,13,2}		
• $K =$	$\frac{1}{ \nabla g ^4} [g_x^2 \cdot (g_{yy}g_{zz} - g_{yz}^2) + 2g_y g_z \cdot (g_{xz}g_{xy} - g_{xx}g_{yz}) + g_y^2 \cdot (g_{xx}g_{zz} - g_{xz}^2) + 2g_x g_z \cdot (g_{yz}g_{xy} - g_{yy}g_{xz}) + g_z^2 \cdot (g_{xx}g_{yy} - g_{xy}^2) + 2g_x g_y \cdot (g_{xz}g_{yz} - g_{zz}g_{xy})]$	
• $K^* =$	$k_K \cdot \nabla g ^4$	
Approach "Förstner/Rohr" ^{6,9,11}		
• $Op3 =$	$\frac{\det(\underline{C})}{\text{trace}(\underline{C})}$	
• $Rohr3D =$	$\det(\underline{C})$	
• $Foerstner3D =$	$\frac{1}{\text{trace}(\underline{C}^{-1})} = \frac{\det(\underline{C})}{\text{trace}(\underline{C}^{adj})}$	with $\underline{C} = \overline{\nabla g(\nabla g)^T}$
Approach "Beaudet" ¹		
• $Beaudet3D =$	$\det(H_g)$	H_g Hessian matrix

Table 1. The investigated nine 3D differential operators classified into four different approaches

2. 3D OPERATORS FOR THE DETECTION OF 3D POINT LANDMARKS

We investigate nine 3D differential operators for detecting anatomical point landmarks in 3D images $g(x, y, z)$ as summarized in Tab.1. All operators are differential operators, and are based on partial derivatives of an image up to second order. Since most of these operators are 3D extensions of 2D corner operators we denote them by the corresponding authors, who introduced the 2D operators, together with the suffix 3D. Three of the nine operators are based on the mean curvature H of isocontours (H , $Kitchen\&Rosenfeld3D$, and $Blom3D$)^{8,3,5,13,11} and two operators are based on the Gaussian curvature K (K and K^*)^{5,13,2}. The operators according to one approach differ only by the exponent of the gradient magnitude. For example, the operator $Blom3D$ results from multiplying the operator $Kitchen\&Rosenfeld3D$ with the second power of the gradient magnitude. Another three operators ($Op3$, $Rohr3D$, and $Förstner3D$)^{6,9,11} are based on the matrix $\underline{C} = \overline{\nabla g(\nabla g)^T}$ with $\nabla g = (g_x, g_y, g_z)^T$ and have been summarized under the approach "Förstner/Rohr". Note, that the latter three operators only require first order partial derivatives of an image. One operator exploits the Hessian matrix H_g (operator $Beaudet3D$)¹.

3. MEASURES FOR THE DETECTION PERFORMANCE

To compare the detection performance of the operators we use different measures. We investigate the number of corresponding points as well as statistical measures.

3.1. Number of corresponding points

The detected points should be both invariant w.r.t deformations and robust against noise. Thus, we should detect the same points if we deform the images or add noise to the images. In our study we investigate the stability w.r.t. deformations by deforming the images with an elastic transformation,^{4,12} while determining automatically the corresponding points in the original image and the deformed image. The transformation is determined by a set of point pairs, while corresponding positions are obtained by applying a random generator. To be more independent of a specific deformation, we deform the images three times and count the number of corresponding points in all of these images. For the case of stability w.r.t. noise we investigate three different levels of Gaussian noise.

3.2. Statistical measures

We use three different statistical measures to investigate how reliably the operators detect landmarks. For each landmark within a ROI (e.g. $25 \times 25 \times 25$ voxels) we use a detection region ($7 \times 7 \times 7$ voxels), which has the advantage that small localization errors of the operators (cf.^{10,7}) do not falsify the detection performance. If at least one detection is within this region, we consider the landmark to be detected and the detected point being a "correct

detection”. If no detection is inside the detection region, we have a “mis-detection” (false negative), whereas if more than one detection is inside the detection region, the landmark is “multiply detected”. A detected point outside the detection region is called a “false detection” (false positive). After application of the operators we determine the overall number of detections (n_d), the number of the correct detections ($n_{d,in}$), and the number of detected landmarks ($n_{l,detect}$). The overall number of landmarks is denoted by n_l . Based on these quantities we compute the following measures of the detection performance:

$$P_{in} = \frac{n_{d,in}}{n_d}, \quad P_{detect} = \frac{n_{l,detect}}{n_l}, \quad P_{multiple} = \frac{n_{d,in}}{n_l}, \quad (1)$$

which quantify the fraction of correct detections, the fraction of detected landmarks, and the average number of multiple detections per landmark, resp. Previously, statistical measures have been applied in the case of 2D corner operators (Zuniga and Haralick¹⁵). There only two measures have been employed and detection regions around corners have not been considered. Thus, the resulting detection performance in that work depends more strongly on the localization accuracy. Using the measures from above we can compute other measures as well, e.g. the average number of detections per landmark:

$$\frac{P_{multiple}}{P_{in}} = \frac{\frac{n_{d,in}}{n_l}}{\frac{n_{d,in}}{n_d}} = \frac{n_d}{n_l}.$$

4. PARAMETER SETTINGS AND IMAGE DATA

The partial derivatives of the images are estimated by applying 3D extensions of the 2D filters of Beaudet¹ with size $5 \times 5 \times 5$ voxels. The components of the matrix \underline{C} of the approach ”Förstner/Rohr”^{6,9,11} are determined by averaging the first order partial derivatives within an observation window of width 3. Extrema of the operator responses are determined by a local maximum and minimum search in $5 \times 5 \times 5$ neighborhoods. We only consider those extrema, whose absolute value is larger than 1% of the largest operator response for the different operators.

The operators are applied to 3D synthetic and 3D tomographic images. The 3D synthetic images include tetrahedra (aperture angles $\beta = 30^\circ, 40^\circ, 50^\circ, 60^\circ, 70^\circ, 80^\circ, 90^\circ$), ellipsoids (lengths of the half axes $a = 8, 9, 10, 11, 12, 13, 14, 15, 16, b = 8, c = 40$), and hyperbolic paraboloids (parameters $(a, b) = (1,1), (2,2), (3,3), (1,2), (1,3), (2,3)$), which are smoothed by a Gaussian function with the standard deviation $\sigma = 0.7$. The tips of the tetrahedra, the tips of the ellipsoids, and the saddle points of the hyperbolic paraboloids are defined as the landmarks. In total we have 22 synthetic 3D images. As 3D tomographic images we use four MR and one CT image. In each of the images we consider 10 landmarks and define ROIs of size $25 \times 25 \times 25$ voxels around each landmark. As anatomical landmarks we use the tips of the frontal, occipital, and temporal horns of the ventricular system, the tip of the external occipital protuberance, the saddle point at the zygomatic bone, and the junction at the upper end of the pons. We have manually specified the positions of these landmarks in the investigated data sets and have taken them as ”ground truth” positions, although we know that manual localization of 3D landmarks generally is difficult and may be prone to error. Since seven of the 50 landmarks are located too close to the border of the image, in total only 43 ROIs (subimages) of the tomographic images could be used.

5. ANALYSIS OF THE OPERATOR VALUES

Fig.1 shows the orthogonal sectional views of the operator values for all nine 3D operators applied to a landmark in a synthetic image (ellipsoid) with added Gaussian noise ($\sigma_n^2 = 100$). It can be seen that the operators H and K are so sensitive to noise such that the landmark (the tip of the ellipsoid) is not recognizable in the operator values. In contrast, the operators $Kitchen\&Rosenfeld3D$, $Blom3D$, and K^* yield a significantly better result. Note that these operators differ from H and K , resp., by multiplication with a certain power of the gradient magnitude. It can also be seen that for the operator $Kitchen\&Rosenfeld3D$ the noise influence is relatively strong everywhere in the image, while for the operators $Blom3D$ and K^* the noise influence is smaller. The operator $Beaudet3D$ yields two extrema at the landmark: a minimum and a maximum (see also, e.g., Rohr¹⁰). The operators $Kitchen\&Rosenfeld3D$, $Blom3D$, K^* , and $Beaudet3D$ detect not only the landmark, but also a larger part of the surface of the ellipsoid. In comparison, for the operators of the approach ”Förstner/Rohr” (operators $Op3$, $Rohr3D$, and $Förstner3D$), the operator values are better concentrated at the tip, and also the noise influence is smaller.

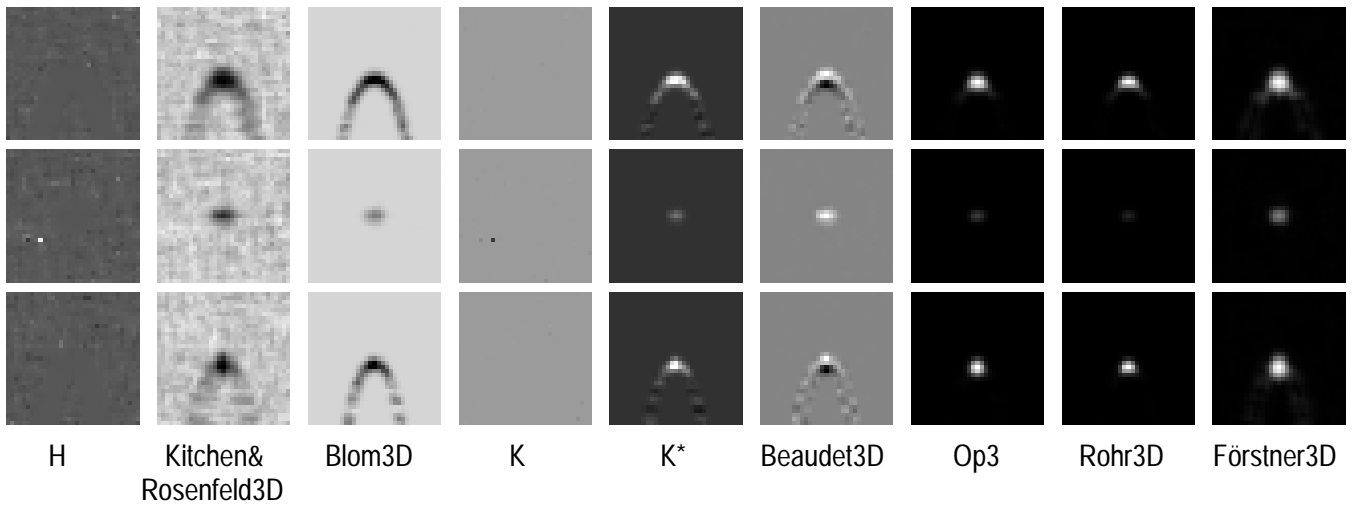


Figure 1. Operator values for an ellipsoid ($a = 10, b = 8, c = 40$) for all nine 3D operators
The figures depict in each column the orthogonal sectional views of the operator values at the landmarks (tip of the ellipsoid). The image has been distorted with Gaussian noise of variance $\sigma_n^2 = 100$.

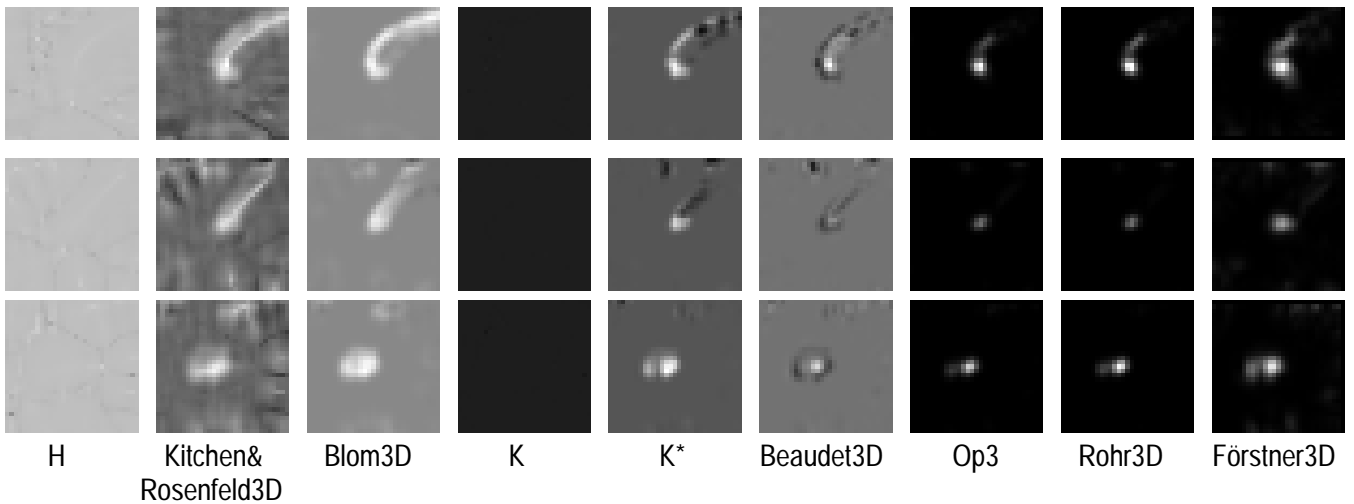


Figure 2. Operator values for a 3D MR image for all nine 3D operators
The figures depict in each column the orthogonal sectional views of the operator values at the landmark "frontal ventricular horn". The rows show the sagittal, axial, and coronal views of all nine 3D operators.

In Fig.2 the operator values at a landmark in a 3D MR image (tip of the left frontal horn of the ventricular system) are shown. The results are comparable to the results for the synthetic image above. In comparison to the operator *Kitchen&Rosenfeld3D* the operators *Blom3D* and *K** emphasize the surface of the ventricular system and better suppress other structures in the image. As above, the operator *Beaudet3D* yields two extrema at the landmark. The operators of the approach "Förstner/Rohr" yield significant values at the landmark and well suppress other structures. In particular for the operators *Op3* and *Rohr3D* the operator values are better concentrated at the landmark in comparison to the other operators.

6. NUMBER OF CORRESPONDING POINTS

To investigate the stability of the operators w.r.t. deformations and noise, we count the number of corresponding points in two images. First we present the principal strategy and then the results of the investigation.

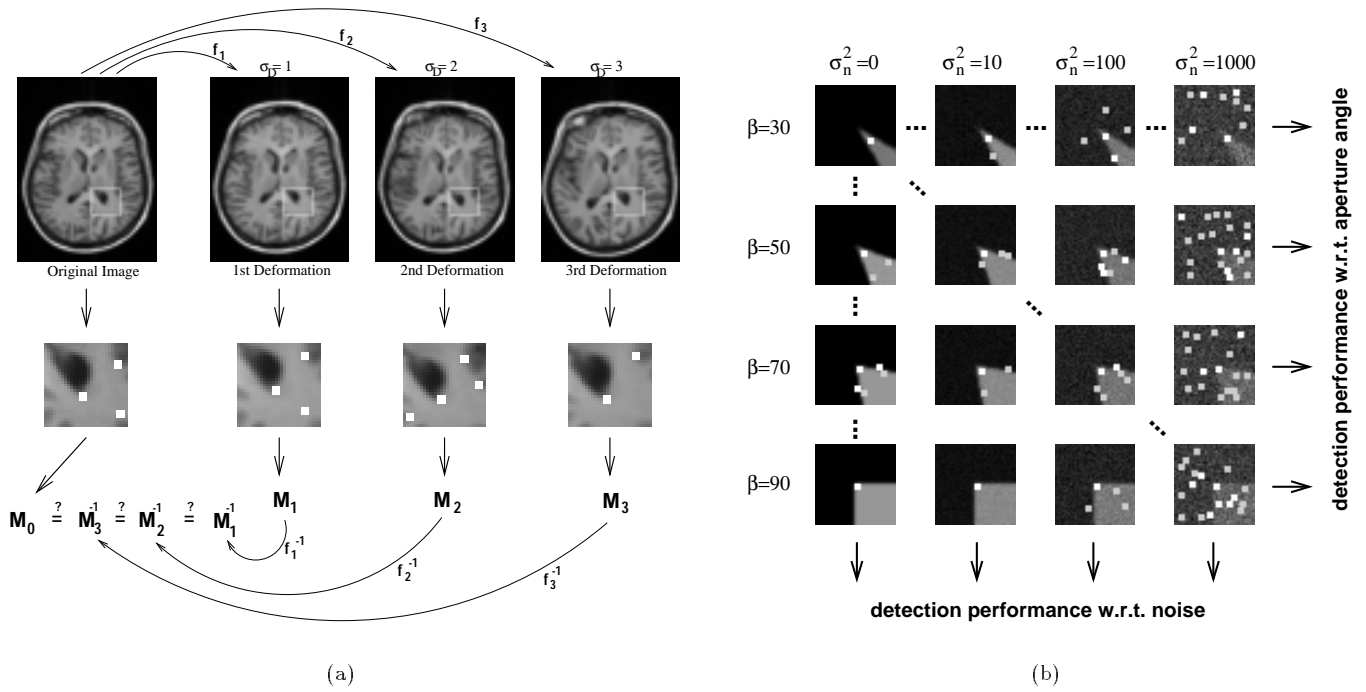


Figure 3. Principal strategies to determine the "number of corresponding points" under elastic deformations (a) and the "statistical performance measures" for synthetic images (b). Fig.3(b) shows the detections of the operator Förstner3D in 3D images of tetrahedra for different noise levels and different aperture angles. Note, that the detections marked in white are within the displayed slice, while the detections marked in grey are in adjacent slices.

6.1. Strategy

We illustrate the principal strategy for the case of deformations (see Fig.3(a)). The 3D images are elastically deformed (by applying thin-plate splines^{4,12}) three times while using a random generator to determine target landmarks (see also Sec.3.1). In Fig.3(a) the transformations are denoted by f_1 , f_2 and f_3 . For each landmark in the original as well as in the deformed images we extract a ROI and apply the operators within these ROIs. Each operator yields a set of detections denoted by M_0 , M_1 , M_2 , and M_3 . We transform the positions of the detections in the deformed images backwards using the inverse transformations f_1^{-1} , f_2^{-1} and f_3^{-1} and verify these positions with those of the detections in the original image. For a correct correspondence a deviation within a $3 \times 3 \times 3$ neighborhood is allowed. In the investigation of stability w.r.t. noise we add three levels of Gaussian noise to the image ($\sigma_n^2 = 1, 4, 10$) and also determine the number of corresponding points in the original and the noisy images. In this case an inverse transformation is not necessary.

A problem is that the operators yield a different number of detections. To make the results better comparable, we divide the number of corresponding points by the total number of detections, thus we compute the fraction of corresponding points. For each type of image (tetrahedra, ellipsoids, hyperbolic paraboloids, MR, and CT images) we average the fraction of corresponding points. Counting the different deformations and the different levels of noise, in total we apply all nine operators to 154 synthetic and 301 tomographic (sub)images.

6.2. Results

The diagrams in Fig.4 depict the results of all operators applied to the 3D synthetic images with ellipsoids, to the 3D MR images, and to the 3D CT images. The diagrams in the first row show the results for the noise study, while those in the second row give the results for the case of deformations.

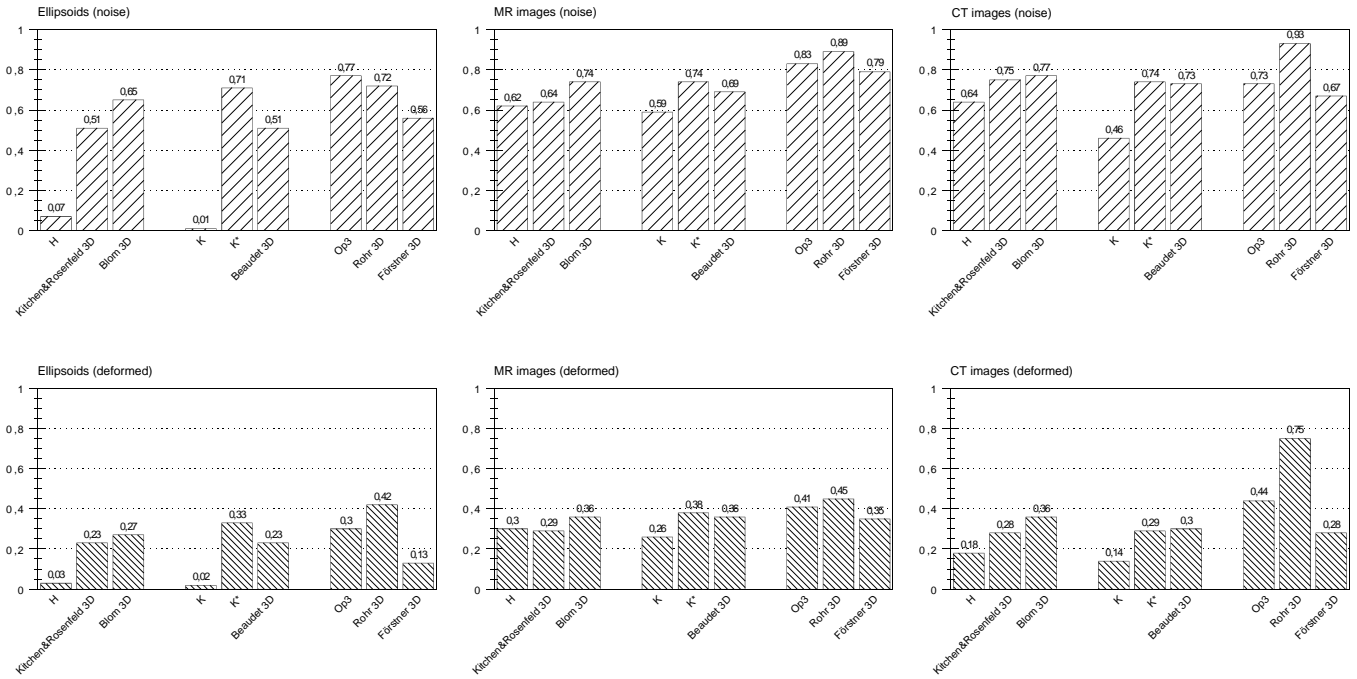


Figure 4. Number of corresponding points (fraction w.r.t. the total number of detections)

6.2.1. Number of corresponding points in noisy images

From Fig.4 (top row, on the left) it can clearly be seen that the operators H and K yield a very small number of corresponding points for synthetic images with added noise. Thus these operators are very sensitive to noise, which is in accordance with the observations in Sec.5. The results for the MR and CT images (Fig.4, top row, in the middle and on the right) are much better (about 60 percent of the detections are corresponding points). However, for the tomographic images the operators H and K yield a very large number of detections, thus many detections seem to correspond by chance. This conjecture will be confirmed through the investigation below using the statistical performance measures. The operators *Kitchen&Rosenfeld3D*, *Blom3D*, and K^* detect always a larger number of corresponding points than the operators H and K . Thus the multiplication with the gradient magnitude improves the results. In particular the operator *Blom3D* yields better results than the operator *Kitchen&Rosenfeld3D*. In all images one of the operators of the approach "Förstner/Rohr" detects the largest number of corresponding points. The operator *Op3* yields the best results for the images with ellipsoids whereas the operator *Rohr3D* yields the best results for the MR and CT images. In comparison to these two operators the operator *Förstner3D* performs slightly worse. The operator *Beaudet3D* yields results worse than the operators *Blom3D* and K^* .

6.2.2. Number of corresponding points in elastically deformed images

In the experiments for elastically deformed images the operators yield a significantly smaller number of corresponding points (second row in Fig.4) than in the case of noisy images. However, the results for the different operators are comparable. The operators H and K only detect a small number of corresponding points in the synthetic images. The multiplication with the gradient magnitude improves the results of the operators of the approach "mean curvature" (H , *Kitchen&Rosenfeld3D*, *Blom3D*) and "Gaussian curvature" (K , K^*). In particular the number of corresponding points of the operator *Blom3D* is larger than that of the operator *Kitchen&Rosenfeld3D*. For the synthetic as well as the tomographic images always one of the operators of the approach "Förstner/Rohr" yields the best results (except for the images with a tetrahedron the result for the operator K^* is better; not displayed here). In the tomographic images the operator *Rohr3D* yields the largest number of corresponding points.

7. STATISTICAL PERFORMANCE MEASURES

The analysis of the operator values (Sec.5) along with the investigation of corresponding points (Sec.6) showed, that the noise influence of the operators differs significantly. In this section, we use the statistical performance measures

described in Sec.3.2 to quantify i) the number of correct detections P_{in} , ii) the number of detected landmarks P_{detect} , and iii) whether the landmarks are multiple detected $P_{multiple}$. We investigate synthetic images with added Gaussian noise as well as MR and CT images.

7.1. Strategy

For each type of images (tetrahedra, ellipsoids, hyperbolic paraboloids, MR, and CT images) the statistical performance measures in (1) are investigated separately. We consider a detection region ($7 \times 7 \times 7$ voxels) around each landmark. If at least one detection is within this region, we consider the landmark to be detected and the detected point being a "correct detection". The principal strategy of the investigation is depicted in Fig.3(b) for the case of tetrahedra. The synthetic images (e.g. for the case of tetrahedra we use aperture angles of $\beta = 30^\circ, 40^\circ, 50^\circ, 60^\circ, 70^\circ, 80^\circ, 90^\circ$) have been disturbed with 10 different levels of Gaussian noise ($\sigma_n^2 = 0.6, 1, 2, 4, 8, 10, 50, 100, 500, 1000$). For each image we determine the measures P_{in} , P_{detect} , and $P_{multiple}$. On the one hand we average the measures for the different parameters of the structure (e.g., in Fig.3(b) we average the results over the columns) and obtain the detection performance w.r.t. these parameters. On the other hand, we average the measures over the different noise levels (e.g., in Fig.3(b) we average the results over the rows) and obtain the detection performance w.r.t. the noise. For the CT and MR images we average the obtained values for the measures over all images (without added noise). In total, in this investigation all nine operators are applied to 242 synthetic and 43 tomographic (sub)images.

7.2. Results

First, we discuss the results for the synthetic images (see Figs.5 and 6 for the case of tetrahedra). Then, we consider the results for the MR and CT images as summarized in Fig.7.

Synthetic images First we consider the total number of detections (dashed line in Fig.5) for the operators of the approach "mean curvature" (H , $Kitchen\&Rosenfeld3D$, and $Blom3D$). In images with added noise the operator H yields a very large number of detections (about 600), which shows that this operator is rather noise sensitive. In the images without noise this operator yields a smaller number of detections, but hardly detects the landmarks ($P_{detect} < 0.2$). For the operator $Kitchen\&Rosenfeld3D$ the number of detections is smaller in images with not much noise ($\sigma_n^2 \leq 1$), but this operator yields as many detections as the operator H in images with a higher level of noise. In comparison to these two operators, the operator $Blom3D$ yields a much smaller number of detections in noisy images. Only in images with a high noise level ($\sigma_n^2 \geq 500$) the number of detections significantly increases to above 200 detections. Thus, all operators of the approach "mean curvature" yield a large number of detections in images with high noise levels, but they differ in the noise level for which the number of detections significantly increases (H : $\sigma_n^2 \approx 0.6$, $Kitchen\&Rosenfeld3D$: $\sigma_n^2 \approx 1$, $Blom3D$: $\sigma_n^2 \approx 500$). Above this noise level the operators detect all landmarks ($P_{detect} = 1$), but yield a small fraction of correct detections ($P_{in} < 0.1$). In this case, the noise influence is that large such that the operators detect points everywhere in the image and thus by chance also in the detection region (e.g., see in Fig.6(b) the detections of the operator $Kitchen\&Rosenfeld3D$ in the last column for the noise level $\sigma_n^2 = 10$). In summary, the comparison of the operators of the approach "mean curvature" applied to noisy images shows that the operator $Blom3D$ is not as sensitive to noise as the operators H and $Kitchen\&Rosenfeld3D$ are.

However, in the images without noise ($\sigma_n^2 = 0$) the operator $Kitchen\&Rosenfeld3D$ detects more landmarks than the operator $Blom3D$ (see Fig.5; $Kitchen\&Rosenfeld3D$: $P_{detect} \approx 0.7$ vs. $Blom3D$: $P_{detect} \approx 0.4$). To illustrate why this is the case, we consider the statistical measures as a function of the aperture angle of the tetrahedra (see Fig.6(a)). While in images with aperture angle $\beta \leq 60^\circ$ the operator $Blom3D$ hardly detects the landmarks ($P_{detect} \approx 0.2$), the operator $Kitchen\&Rosenfeld3D$ detects at least 70% of the landmarks ($P_{detect} \geq 0.7$). The reason is that the localization error of the operator $Blom3D$ is larger than that of the operator $Kitchen\&Rosenfeld3D$. For example, in the image with an aperture angle of $\beta = 50^\circ$ and without noise the operator $Blom3D$ yields no detection at the landmark (compare in Fig.6(b) the detections of the operators $Kitchen\&Rosenfeld3D$ and $Blom3D$ in the first and second column).

We now compare the approach "mean curvature" with the approach "Gaussian curvature" by comparing the operator H and $Blom3D$ with the operators K and K^* , resp. Note that the operators $Blom3D$ and K^* differ from H and K , resp., only by multiplication with a certain power of the gradient magnitude. Fig.5 shows that the operators of the approach "Gaussian curvature" (K , K^*) yield similar results as the operators of the approach "mean curvature" (H , $Kitchen\&Rosenfeld3D$, $Blom3D$). As the operator H the operator K is largely influenced by noise. As with the

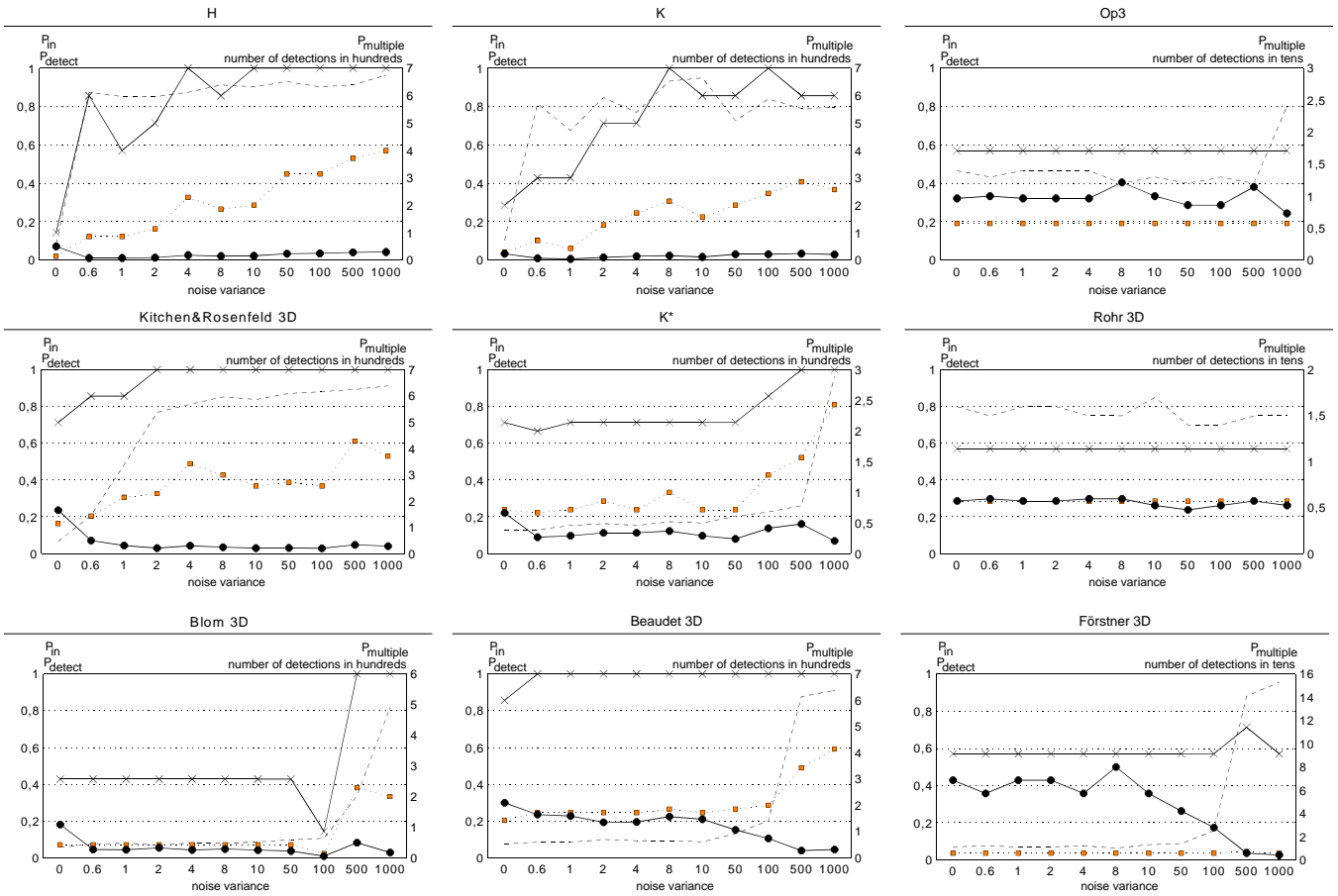
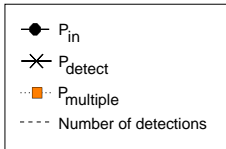


Figure 5. Statistical performance measures for tetrahedra as a function of image noise

The measures P_{in} , P_{detect} , $P_{multiple}$ were averaged over all different aperture angles ($\beta = 30^\circ, 40^\circ, 50^\circ, 60^\circ, 70^\circ, 80^\circ, 90^\circ$) of the tetrahedra. In the diagrams these averaged measures and the number of the detections in all images are depicted. The measures P_{in} and P_{detect} refer to the units on the left side of the diagrams and the measure $P_{multiple}$ and the number of detections refer to the units on the right side of the diagrams (please note that the units must be multiplied by 10 resp. 100).



operator *Blom3D* the noise influence of the operator K^* is smaller in comparison to the operator K (see in Fig.5 the number of detections and in Fig.6(b) the detections of the operator K^* in the noisy image). However, in comparison to the operator *Blom3D* the operator K^* detects more landmarks ($P_{detect} > 0.6$) and yields a larger fraction of correct detections ($P_{in} \approx 0.1$ in noisy images). As one can see in Fig.6(b) first row, in the image with the aperture angle $\beta = 50^\circ$ the localization error of the operator K^* is smaller than that of the operator *Blom3D*.

In comparison to the operators of the approaches "mean curvature" and "Gaussian curvature" the operator *Beaudet3D* yields better results in the images with tetrahedra (Fig.5). Both the fraction of detected landmarks P_{detect} and the fraction of correct detections P_{in} are in general significantly larger.

The operators of the approach "Förstner/Rohr" yield significantly more correct detections (P_{in} is larger) than the operators of the other approaches (see the last column in Fig.5). For example, the operator *Rohr3D* yields at least 20% correct detections ($P_{in} > 0.2$) in images with as well as without noise. Note, that the fraction of correct detections for the operators *Op3* and *Rohr3D* is hardly influenced by noise and the number of detections is at least ten times smaller than the number of detections for the operators of the other approaches. The reason why the operators of the approach "Förstner/Rohr" do not detect all landmarks ($P_{detect} < 1$ in Fig.5) are localization errors for small aperture angles of the tetrahedron (compare with the results of the operator *Blom3D* from above).

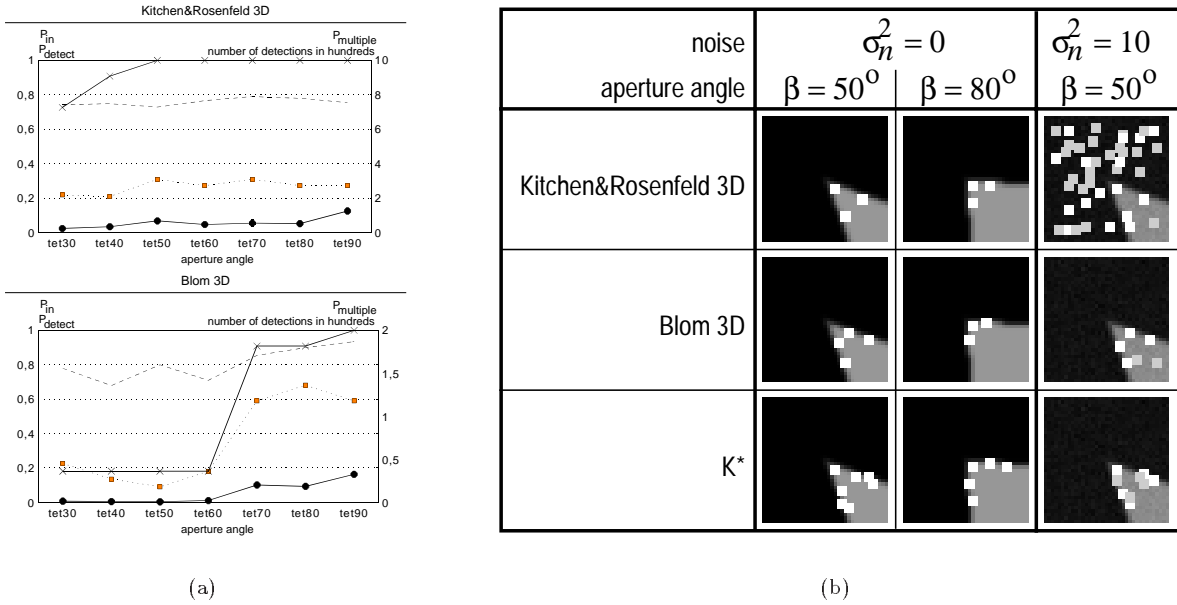


Figure 6. Statistical performance measures for tetrahedra as a function of the aperture angle (a). In (b) the detections of three different operators in images with a tetrahedron are shown.

In Fig.6(a) the measures P_{in} , P_{detect} , $P_{multiple}$ are averaged over different levels of Gaussian noise ($\sigma_n^2 = 0.6, 1, 2, 4, 8, 10, 50, 100, 500, 1000$) and are depicted as a function of the aperture angle ($\beta = 30^\circ, 40^\circ, 50^\circ, 60^\circ, 70^\circ, 80^\circ, 90^\circ$). The units are analogous to Fig.5.

Fig.6(b) depict the detections of the operators *Kitchen&Rosenfeld3D*, *Blom3D*, and *K** in 3D images with and without noise and for different aperture angles $\beta = 50^\circ$ and $\beta = 80^\circ$. The detections marked in white are within the displayed slice, while the detections marked in grey are in adjacent slices.

Tomographic images The results for the MR and CT images are depicted in Fig.7. Note, that the measures P_{in} , P_{detect} , $P_{multiple}$ have been averaged over all investigated MR and CT images. For the MR images (see Fig.7 upper diagram) it can be seen that the operators *Kitchen&Rosenfeld3D*, *K** and *Beaudet3D* detect more landmarks ($P_{detect} \approx 1$) than the operators of the approach "Förstner/Rohr" (e.g., *Op3*: $P_{detect} \approx 0.8$). However, they yield a significant smaller fraction of correct detections (P_{in} is smaller). If both P_{in} and P_{detect} are taken into consideration, the operator *Rohr3D* yields the best results among the operators of the approach "Förstner/Rohr" and the operator *K** yields the best results among the operators of the approaches "mean curvature", "Gaussian curvature", and "Beaudet". We now analyze the results of these two operators in more detail. Since the fraction of correct detections for the operator *Rohr3D* is about 30% ($P_{in} \approx 0.3$) and since on average one detection is inside a detection region ($P_{multiple} \approx 1$), the operator detects $\frac{P_{multiple}}{P_{in}} \approx 3$ points per landmark (see Sec.3.2). Thus, the operator yields per landmark one correct detection ($P_{multiple} \approx 1$) and two false detections. In comparison, the fraction of correct detections for the operator *K** is about 10% ($P_{in} \approx 0.1$) and the average number of multiple detections is $P_{multiple} \approx 2$. Thus, this operator detects about $\frac{P_{multiple}}{P_{in}} \approx 20$ points per landmark, and therefore the operator yields 18 false detections per landmark beside the two correct detections ($P_{multiple} \approx 2$). This comparison shows that the operators of the approach "Förstner/Rohr" (in particular the operators *Op3* and *Rohr3D*) yield a significant smaller number of false detections, thus their detection performance is better.

The comparison of the operators of the approaches "mean curvature" and "Gaussian curvature" shows that the multiplication with the gradient magnitude improves the results. Both the fraction of correct detections P_{in} and the fraction of detected landmarks P_{detect} are higher. In particular, the operator *Blom3D* yields more correct detections than the operator *Kitchen&Rosenfeld3D*. Analogously, *K** performs better than *K*. Note also, that the operators *H* and *K* yield a relatively large number of detections in the tomographic images as we have already mentioned above in Sec.6.2.1.

For the CT images the results of the different operators (Fig.7 bottom diagram) support our findings derived

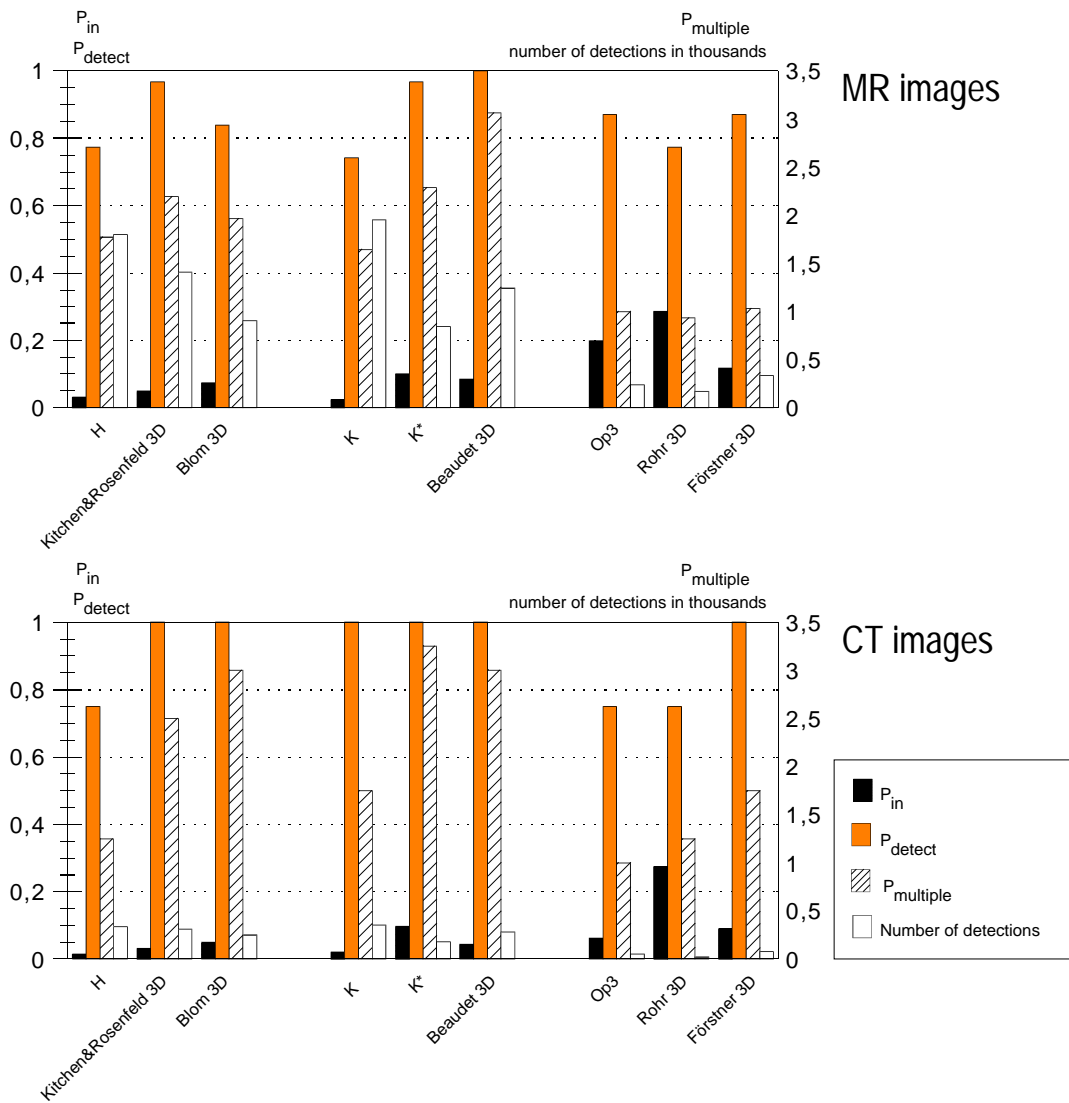


Figure 7. Statistical performance measures for MR and CT images

The measures P_{in} , P_{detect} , $P_{multiple}$ have been averaged over all investigated MR and CT images. Beside these measures the number of detections in all images has been represented in the diagrams. The measures P_{in} and P_{detect} refer to the units on the left side of the diagrams and the measure $P_{multiple}$ and the number of detections refer to the units on the right side of the diagrams.

from the experiments with MR images. However, the operator $Op3$ yields a smaller fraction of correct detection (P_{in} is smaller) than in the case of MR images.

8. CONCLUSION

In this paper, we have investigated the performance of nine 3D operators for the detection of anatomical point landmarks. The operators are summarized in Tab.1. We introduced quantitative measures which represent different aspects of the detection performance. We analyzed the number of corresponding points in images under elastic deformation as well as for different noise levels, and applied statistical measures to determine the detection performance. Altogether each of the nine operators has been applied to 308 synthetic 3D images (tetrahedra, ellipsoids, and hyperbolic paraboloids with different levels of noise and deformations) and 301 tomographic (sub)images (3D ROIs of MR- and CT images also with different levels of noise and deformations; the ROIs have been taken from four MR and one CT image). The results of this investigation can be summarized as follows:

1. The operators of the approach "Förstner/Rohr" ($Op3$, $Rohr3D$, $Förstner3D$) are more stable w.r.t. noise than the operators of the other approaches and thus they yield a smaller number of detections. Besides that, they detect more than 70% of the landmarks in tomographic images ($P_{detect} > 0.7$). Therefore, they generally yield a larger fraction of correct detections P_{in} . Furthermore, either the operator $Op3$ or the operator $Rohr3D$ yields the largest number of corresponding points in deformed and noisy images.
2. Comparing the operators of the approach "Förstner/Rohr" ($Op3$, $Rohr3D$, $Förstner3D$) with each other, it turns out that the operators $Op3$ and $Rohr3D$ are superior. The number of corresponding points in deformed and noisy images as well as the fraction of correct detections P_{in} is generally larger.
3. The multiplication with the gradient magnitude improves the results of the operators H and K as the comparison of the operators of the approaches "mean curvature" (H , $Kitchen\&Rosenfeld3D$, $Blom3D$) and "Gaussian curvature" (K , K^*) showed. The number of corresponding points in deformed and noisy images as well as the fraction of correct detections P_{in} of the operators $Blom3D$ and K^* are larger than those of the operators H and K , resp.

In summary our investigation shows, that the operators based on only first order partial derivatives of an image (operators $Op3$, $Rohr3D$, and $Förstner3D$) yield the best results w.r.t. the number of corresponding points and the statistical measures. Out of these operators, the operators $Op3$ and $Rohr3D$ show superior performance.

Acknowledgment: This work has partially been supported by Philips Research Hamburg, project IMAGINE (IMage- and Atlas-Guided Interventions in NEuroSurgery).

REFERENCES

1. P. Beaudet. Rotationally invariant image operators. In *Proc. 4th Int. Joint Conf. Patt. Recog.*, pages 579–583, November 1978. Kyoto, Japan.
2. W. Beil, K. Rohr, and H.S. Stiehl. Investigation of approaches for the localization of anatomical landmarks in 3D medical images. In *Proc. Computer Assisted Radiology and Surgery (CAR'97)*, pages 265–270, Juni 1997.
3. J. Blom. *Topological and Geometrical Aspects of Image Structure*. PhD thesis, Utrecht University, 1992.
4. F. L. Bookstein. Principal warps: Thin-plate splines and the decomposition of deformations. *IEEE Transactions on Pattern Analysis and Machine Intelligence*, PAMI-11(6):567–585, 1989.
5. L. M. J. Florack, B. M. ter Haar Romeny, J. J. Koenderink, and M. A. Viergever. General intensity transformations and differential invariants. *Journal of Mathematical Imaging and Vision*, 4(2):171–187, 1994.
6. W. Förstner. A feature based correspondence algorithm for image matching. In *Int. Arch. Photogramm. Remote Sensing*, volume 26, pages 150–166, 1986.
7. S. Frantz, K. Rohr, and H.S. Stiehl. Refined Localization of Three-Dimensional Anatomical Point Landmarks Using Multi-Step Differential Approaches. In *Proc. SPIE's International Symposium Medical Imaging, Image Processing*, pages 28–38, San Diego, CA, USA, 1998.
8. L. Kitchen and A. Rosenfeld. Grey level corner detection. *Pattern Recognition Letters*, 1:95–102, December 1982.
9. K. Rohr. Untersuchung von grauwertabhängigen Transformationen zur Ermittlung des optischen Flusses in Bildfolgen. *Diplomarbeit, Institut für Nachrichtensysteme, Universität Karlsruhe, Germany*, 1987.
10. K. Rohr. Localization properties of direct corner detectors. *Journal of Mathematical Imaging and Vision*, 4(2):139–150, 1994.
11. K. Rohr. On 3D differential operators for detecting point landmarks. *Image and Vision Computing*, 15(3):219–233, March 1997.
12. K. Rohr, H. S. Stiehl, R. Sprengel, W. Beil, T.M. Buzug, J. Weese, and M.H. Kuhn. Point-based elastic registration of medical image data using approximating thin-plate splines. In K.H. Höhne and R. Kikinis, editors, *Proc. 4th Internat. Conf. Visualization in Biomedical Computing (VBC'96)*, volume 1131 of *Lecture Notes in Computer Science*, pages 297–306, Sept. 1996.
13. J. P. Thirion and A. Gourdon. Computing the differential characteristics of isointensity surfaces. *Computer Vision and Image Understanding*, 61(2):190–202, March 1995.

14. J.P. Thirion. New feature points based on geometric invariants for 3d image registration. *Intern. J. of Computer Vision*, 18(2):121–137, May 1996.
15. O. A. Zuniga and R. M. Haralick. Corner detection using the facet model. In *Proc. IEEE Conf. on Computer Vision and Pattern Recognition*, pages 30–37, 1983.